# THEORY OF ELECTRON- AND PHOTON-INDUCED TWO-ELECTRON EMISSION FROM SURFACES

Roland Feder, Herbert Gollisch, and Thomas Scheunemann
*Theoretische Festkörperphysik, Universität Duisburg*
*D-47048 Duisburg, Germany*

Jamal Berakdar and Jürgen Henk
*Max-Planck-Institut für Mikrostrukturphysik*
*Weinberg 2, D-06120 Halle (Saale), Germany*

**Abstract** A short review is given of recent theoretical developments in (e,2e) and ($\gamma$,2e) spectroscopy from surfaces in reflection geometry. We first outline a general formal framework and currently viable approximations. Subsequently, a selection of numerical results demonstrates the quantitative agreement with experimental data, the extreme surface sensitivity of (e,2e), the imaging of a surface state dispersion, the influence of the Coulomb pair correlation between the two detected electrons, and the usefulness of spin-polarized primary electrons for the study of spin-dependent collision dynamics and of magnetic surface properties.

**Keywords:** Two-electron emission, surfaces, magnetism

## 1. INTRODUCTION

Over the past few years, there have been substantial experimental advances in the energy- and momentum-resolved detection of pairs of time-correlated electrons, which are emitted from solid surfaces after electron or photon impact. For recent experimental highlights and references to earlier (e,2e) and ($\gamma$,2e) spectroscopy studies, we refer the reader to articles published in this same volume, in particular those by Kirschner and Samarin, 2001, Stefani, 2001, and Weigold, 2001.

The understanding of the physical mechanisms, the quantitative interpretation of experimental data and the pointing out of future directions have been the aims of a variety of theoretical investigations. In this

*Many-Particle Spectroscopy of Atoms, Molecules, Clusters, and Surfaces*, edited by Berakdar and Kirschner, Kluwer Academic/Plenum Publishers, New York 2001

article, we briefly review the current status of the theory of (e,2e) and ($\gamma$,2e) spectroscopies from surfaces in the reflection geometry.

In Section 2, we outline the theoretical framework in terms of genuine two-electron states and address approximate reductions to one-electron quantities. In Section 3, a representative selection of theoretical (e,2e) results is discussed in contact with experimental data, with topical focuses on sensitivity to the surface electronic structure (in particular surface states), on the scattering mechanisms, on the Coulomb correlation between the two detected electrons, and on the use of spin-polarized primary electrons for studying spin-orbit coupling effects and ferromagnetic surface properties. Results for photon-induced two-electron emission are presented in Section 4.

## 2. FORMAL FRAMEWORK

Dealing first with (e,2e), we recall (Fig. 1) that after the collision of a primary electron (which we characterize by the label 1) with a valence electron of the solid (labeled as 2), two electrons (labeled as 3 and 4) leave the surface in the directions of the detectors.

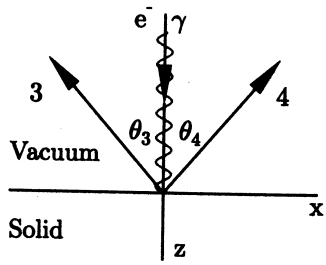


*Figure 1* Typical geometry of (e,2e) and ($\gamma$,2e) spectroscopy from a surface. Upon normal impact of an electron or a photon, two electrons (labeled as 3 and 4, see text) are emitted in the directions of the detectors.

The initial asymptotic state of the system is thus an anti-symmetrized direct product of two single quasi-particle states, i.e. $|1,2\rangle = |1\rangle \otimes |2\rangle$. The states $|1\rangle$ and $|2\rangle$ are solutions of a Dirac equation involving optical potentials $V_1$ and $V_2$, respectively, which incorporate the interaction with the nuclei and all the other ground state electrons. For a crystalline system with lattice periodicity parallel to the surface, the relativistic one-electron states $|i\rangle$ are characterized by energies $E_i$, surface-parallel two-dimensional wave vectors $\boldsymbol{k}_i^{\parallel}$ and spin labels $\sigma_i$. The number $i$ in $|i\rangle$ is thus an abbreviation for the set of quantum numbers $(E_i, \boldsymbol{k}_i^{\parallel}, \sigma_i)$. For the relativistic LEED (low-energy electron diffraction) state $|1\rangle$, the set $(E_1, \boldsymbol{k}_1^{\parallel}, \sigma_1)$ is dictated by the experimental conditions and is equivalent to the three-dimensional wave vector $\boldsymbol{k}_1$ and the spin alignment at the electron gun. Even if the primary beam is unpolarized, states $|1\rangle$ with

$\sigma_1 = \pm$ have to be employed and finally summed over. The same holds in any case for the valence states $|2\rangle$.

For the electron-electron interaction $U$ considered as a perturbation, standard scattering theory gives the transition amplitude for the initial state $|1,2\rangle$ to go over into the two-electron excited state $|3,4\rangle$ as $\langle 3,4|U|1,2\rangle$. Strictly speaking, $|3,4\rangle$ is an eigenstate of a two-electron Dirac equation involving the total potential $V_{\rm tot} = V_3 + V_4 + U$, where $V_3$ and $V_4$ are one-particle optical potentials, and with asymptotic boundary conditions such that an electron with momentum $\boldsymbol{k}_3$ and spin alignment $\sigma_3$ arrives at one detector and an electron with momentum $\boldsymbol{k}_4$ and spin alignment $\sigma_4$ at the other detector.

The (e,2e) transition rate is then the absolute square of the matrix element $\langle 3,4|U|1,2\rangle$. If one describes the valence electron by a retarded single-particle Green function $G_2^{\rm r}$, one obtains the more general expression

$$\langle 3,4|U|1\rangle\,(-1/\pi)\mathrm{Im}\,G_2^{\rm r}\,\langle 1|U|3,4\rangle\,. \tag{1}$$

The above implicitly contains the conservation laws

$$E_1 + E_2 = E_3 + E_4 \quad \text{and} \quad \boldsymbol{k}_1^{\parallel} + \boldsymbol{k}_2^{\parallel} = \boldsymbol{k}_3^{\parallel} + \boldsymbol{k}_4^{\parallel}, \tag{2}$$

where $\boldsymbol{k}_2^{\parallel}$ is determined modulo a surface reciprocal lattice vector $\boldsymbol{g}^{\parallel}$. The trace of the spectral function in the middle of eq. (1) is the spin- and $k^{\parallel}$-resolved density of states $N(E_2, \boldsymbol{k}_2^{\parallel}, \sigma_2)$.

Wishing to evaluate $\langle 3,4|U|1,2\rangle$ and eq. (1), one faces the severe difficulty of solving a two-electron equation containing the non-separable potential $V_{\rm tot}$. The simplest and most frequently used approximation is to neglect the electron-electron interaction term $U$. The state $|3,4\rangle$ then reduces to an anti-symmetrized direct product of two independent time-reversed LEED states, $|3\rangle$ and $|4\rangle$. These can be readily calculated by the layer-KKR method routinely employed in LEED and photoemission calculations (Feder, 1985; Halilov et al., 1993). All elastic multiple-scattering events by the ion-core lattice, i.e. loosely speaking 'band structure effects', are thereby taken into account. An approximate incorporation of $U$ was recently put forward by Berakdar et al., 1999, by transforming it into two one-electron potential parts $v_3$ and $v_4$ such that $v_3$ depends on the crystal momentum of electron 4 and vice versa. This amounts to a dynamical screening of the original optical potentials $V_3$ and $V_4$. The one-electron equations containing these screened potentials can be solved by the standard layer-KKR method to yield modified states $|3\rangle$ and $|4\rangle$, which are again combined into an anti-symmetrized product.

With either of the above two approximations, $\langle 3,4|U|1,2\rangle$ has the form $f-g$, where the direct scattering amplitude $f$ is

$$f_{\sigma_1,n\sigma_2,\sigma_3,\sigma_4} = \int \psi_3^{\sigma_3\star}(\boldsymbol{x})\psi_4^{\sigma_4\star}(\boldsymbol{x}')V(\boldsymbol{x},\boldsymbol{x}')\psi_1^{\sigma_1}(\boldsymbol{x})\psi_2^{n\sigma_2}(\boldsymbol{x}')\,\mathrm{d}^3x\,\mathrm{d}^3x' \quad (3)$$

and the expression for the exchange scattering amplitude $g$ is the same except for $\boldsymbol{x}$ and $\boldsymbol{x}'$ interchanged in the first product term. In the notation of the one-electron wave functions $\psi$, the state subscripts $i$ comprise the quantum numbers $E_i$ and $\boldsymbol{k}_i^{\parallel}$ and the superscripts $\sigma_i$ are the spin labels; the additional superscript $n$ in $\psi_2^{n\sigma_2}$ enumerates the independent valence states of the semi-infinite system, which are associated with outgoing bulk Bloch waves (for details see Feder et al., 1998). For primary electrons with spin orientation $\sigma_1$ relative to an axis $\boldsymbol{e}$ (i.e. spin polarization vector $\boldsymbol{P}_1 = \sigma_1\boldsymbol{e}$) and fixed energy and momentum, and for spin-unresolved detection of the outgoing electrons in fixed directions, this leads to the following expression for the (e,2e) cross section ('intensity'):

$$\begin{aligned} I^{\sigma_1} &= \frac{k_3k_4}{k_1}\sum_{\sigma_3,\sigma_4}\sum_{E_2,\boldsymbol{k}_2^{\parallel},n\sigma_2} |f_{\sigma_1,n\sigma_2,\sigma_3,\sigma_4} - g_{\sigma_1,n\sigma_2,\sigma_3,\sigma_4}|^2 \\ &\times\ \delta(E_1+E_2-E_3-E_4)\delta(\boldsymbol{k}_1^{\parallel}+\boldsymbol{k}_2^{\parallel}-\boldsymbol{k}_3^{\parallel}-\boldsymbol{k}_4^{\parallel}). \end{aligned} \quad (4)$$

Since the spin of the outgoing electrons is presently not resolved, the observed cross section is the $(\sigma_3,\sigma_4)$ sum over cross sections involving states $\psi_3^{\sigma_3}$ and $\psi_4^{\sigma_4}$. Each of these partial cross sections consists of a sum over the independent valence states. $V(\boldsymbol{x},\boldsymbol{x}')$ in eq. (3) approximates the electron-electron interaction $U$ by the Coulomb interaction statically screened by the ground state electrons of the target: $V(\boldsymbol{x},\boldsymbol{x}') = \int d^3x''\epsilon^{-1}(\boldsymbol{x},\boldsymbol{x}'')/|\boldsymbol{x}''-\boldsymbol{x}'|$, where $\epsilon(\boldsymbol{x},\boldsymbol{x}'')$ is the dielectric function of the crystalline surface system.

The more general transition rate expression eq. (1) can be evaluated along similar lines, yielding rather lengthy expressions for the intensities $I^{\pm}$ (Meinert, 2000). This approach is computationally much more demanding than the matrix-element formulation in eq. (4), but has two advantages: the imaginary self-energy part, which describes the lifetime of the valence-band hole, can be incorporated from the start, and surface states, which are very hard to find via eq. (4), are reliably and conveniently accessible.

An asymmetry $A$ of the cross section upon reversal of the primary electron spin is defined from the intensities $I^{\pm}$ in $\langle 3,4|U|1,2\rangle$ as $A = (I^+-I^-)/(I^++I^-)$. If spin-orbit coupling is neglected in all four states,

the spinor wave functions reduce to products of a scalar wave function with a basis spinor. For non-magnetic surface systems, one then obtains $I^+ = I^-$, and therefore $A = 0$. For ferromagnetic systems, however, the spatial wave functions for majority and minority spin (at the same $E_2$ and $\boldsymbol{k}_2^{\parallel}$) differ from each other and one generally obtains a non-zero exchange-induced asymmetry $A$. If spin-orbit coupling is taken into account, it produces a non-zero $A$ already for non-magnetic systems.

In ($\gamma$,2e) spectroscopy from surfaces, the main process is the direct excitation of an electron pair by the incident photon of energy $\omega$. The resulting photocurrent is in first order perturbation theory (in the electron-photon interaction, which at photon energies below about 100 eV is adequately described by the two-particle dipole operator $\Delta$) given by the golden-rule form (Berakdar, 1998)

$$\sum_j |\langle\Psi|\Delta|\Phi_j\rangle|^2 \delta(E - \omega - E_j), \tag{5}$$

where the final state $|\Psi\rangle$ with energy E is identical with the above (e,2e) final state $|3,4\rangle$. $|\Phi_j\rangle$ denotes occupied two-particle states with energies $E_j$ and further quantum numbers comprised by the index $j$. The summation over $j$ accounts for all initial two-particle states that are compatible with energy conservation and dipole transition selection rules. The dipole operator $\Delta$ is the sum of two single-particle dipole operators, and the conservation of the surface-parallel component of the momentum in one-electron photoemission transforms in two-electron photoemission into the same requirement for the two-particle momentum $\boldsymbol{K}^{\parallel}$. For a more general photocurrent expression in terms of two-particle Green functions we refer to Fominykh et al., 2000, and Fominykh et al., 2001.

As the most important property of the 2e-photocurrent eq. (5) we point out that it vanishes in a single-particle picture, i.e. if both two-particle states are approximated by anti-symmetrized products of independent single-particle states (forming an orthonormal set; cf. Berakdar, 1998). This implies that ($\gamma$,2e) spectroscopy is most suitable for studying the Coulomb correlation in solid surface systems. In to-date calculations, $U$ has only been taken into account in the two-particle final state in approximate ways (cf. above in the context of (e,2e) and Berakdar et al., 1998; Fominykh et al., 2001).

In addition to the above one-step process, another process has been found to contribute to the observed 2e-photocurrent (Herrmann et al., 1998; Herrmann et al., 1999; Berakdar, 1998) which consists of two steps: *(i)* The photon of frequency $\omega$ is absorbed by a single valence electron. *(ii)* The resulting hot electron scatters from another valence electron, and the two electrons then leave the crystal.

## 3. (e,2e) RESULTS

As for high-energy (e,2e) studies in transmission geometry, which have their main potential in the study of bulk-like electronic properties, we restrict ourselves to a few remarks and refer the reader to the review by Weigold, 2001, and the monographs Whelan and Walters, 1997, and Weigold and McCarthy, 1999. Incoming and outgoing electrons with energies of the order of 10 keV can be described by independent plane waves, which reduces the observed cross section (cf. eq. (1)) to the valence or core electron spectral function in momentum space. If multiple inelastic events can be sufficiently dealt with, the experimental data can be directly compared with calculated spectral functions. Recently, such comparison was shown to be able to discriminate between several theoretical approaches (Vos et al., 1999), favouring the so-called cumulant expansion, a very advanced many-body method.

We now proceed to a selection of recent theoretical results for low-energy (e,2e) in reflection geometry. Fig. 2 shows a typical intensity dis-

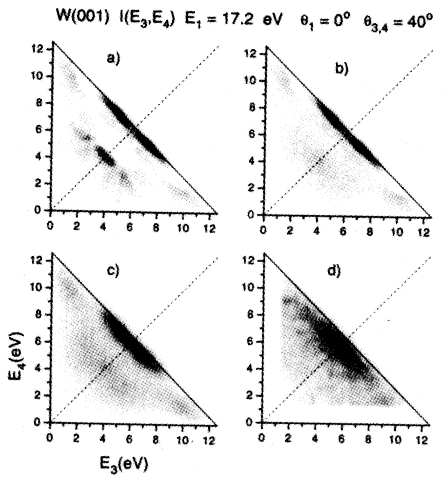


*Figure 2* (e,2e) from W(001) with normally incident unpolarized primary electrons of energy $E_1 = 17.2\ eV$ and detection of the outgoing electrons in the $(xz)$ plane at polar angles $\theta_3 = \theta_4 = 40°$. The contour plots show the (e,2e) intensity as a function of the energies $E_3$ and $E_4$ of the outgoing electrons: (a) calculated at sharp $E_1$, $\theta_3$ and $\theta_4$ assuming an infinite lifetime of the valence band hole; (b) like (a) but with finite hole lifetime; (c) calculated with finite hole lifetime and averaged over the experimental $E_1$ distribution and the 22° acceptance cones of the detectors; (d) experiment. In each plot, the dashed diagonal line marks equal energies of the outgoing electrons; as is evident from energy conservation (eq. (2)), the electrons along the solid counter-diagonal originate from collisions with valence electrons with energy $E_2 = E_F$ (Fermi level) (cf. Feder et al., 1998).

tribution (as a function of the outgoing electron energies $E_3$ and $E_4$ at fixed geometry and primary electron energy) in its evolution from ideal theory to experimental reality. The two-electron state $|3,4\rangle$ was approximated by an anti-symmetrized product of one-electron states, which were calculated by the relativistic layer-KKR method as time-reversed LEED states. The contour plots in Fig. 2 are seen to be symmetric with respect to the $E_3 = E_4$ diagonal, which is a consequence of the symmetry of the geometrical set-up. In Fig. 2a, which was obtained assuming an infinite hole lifetime, dominant intensity features occur at ($E_3$, $E_4$) around (7 eV, 6 eV) and (6 eV, 7 eV). From energy conservation (cf. eq. (2)), they can be seen to originate from valence electrons very close to the Fermi energy. Taking into account finite hole lifetime (described by an imaginary potential part, which is very small at $E_F$ and increases with increasing binding energy)(see Fig. 2b), the mentioned features near $E_F$ are hardly affected, whereas features at higher binding energies are strongly reduced and smeared out. Upon averaging over the acceptance cones of the detectors (Fig. 2c), the two features near $E_F$ merge and overall agreement with the experimental data (Fig. 2d) is reached.

The decomposition of the intensity in Fig. 2 into contributions from atomic layers parallel to the surface (see upper half of Fig. 3) reveals that more than 80% comes from the topmost layer. Note that the above is for normal incidence of the primary electron. For grazing incidence, the relative contributions from the second and third layers are even smaller. In comparison, LEED and photoemission spectra typically have substantial contributions from up to five layers. This extreme surface sensitivity of the (e,2e) process is plausible from the fact that the matrix elements involve three states decaying into the crystal (one LEED state and two time-reversed LEED states), whereas in LEED and in photoemission there is only one such state. In the lower half of Fig. 3 we show the layer-resolved density of valence states $N_l(E_2, k_{2x})$, i. e. the central term in the cross section expression eq. (1). In contrast to $N_3$, which is already bulk-like, $N_1$ is seen to be sizable at the energies of the dominant intensity features. This corroborates the surface sensitivity. The weak (e,2e) intensities associated with other regions of large $N_1$ indicate the importance of matrix elements effects. The (e,2e) intensity is thus in general not a direct image of the spectral function in the surface layer. This may however be the case, as we will now demonstrate for a surface state.

Fig. 4 is devoted to the sp-like surface state on Cu(111), which is well known from one-electron photoemission studies and is found in textbooks as a surface-state paradigm. It is seen, for $\boldsymbol{k}^{\parallel} = 0$, in the upper left-hand panel of Fig. 4 in the first layer density of states as the peak

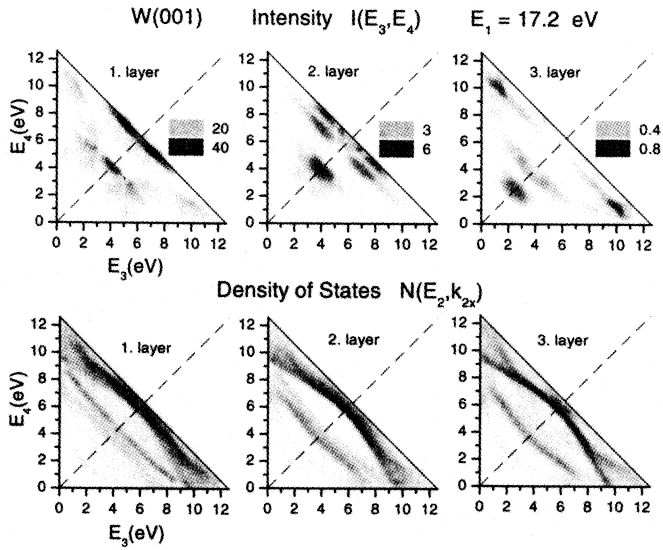


*Figure 3* *Upper half*: Contributions to the calculated (e,2e) intensity in Fig. 2a from the first three mono-atomic layers parallel to the surface. The numbers to the right of the grey-scale rectangles indicate the intensity values in the respective panels. *Lower half*: $\boldsymbol{k}^{\|}$-resolved valence electron density of states (cf. eq. (1)) in the first three layers. Due to energy and parallel momentum conservation (eq. (2)), each pair $(E_3,E_3)$ uniquely corresponds to a pair $(E_2,k_{2x})$, all $k_{iy}$ being zero in the present coplanar geometry (cf. Meinert, 2000).

labelled SS, which resides at 0.4 eV below $E_F$ in the sp-like bulk-band gap along $\Gamma$–$L$. Comparison of the (e,2e) intensity calculated for exit angles $\theta_3 = \theta_4 = 45°$ (lower panel) with the corresponding first layer density of states $N_l(E_2, k_{2x})$ (upper right-hand panel) shows that (e,2e) spectroscopy directly reflects the surface state and its dispersion. For exit angles 30° and 60°, the dispersion of the (e,2e) image is seen to widen and to narrow, respectively. This is readily understandable from the conservation relations in eq. (2).

The Coulomb correlation between the two outgoing electrons, which corresponds to the deviation of the actual two-electron state $|3,4\rangle$ from an anti-symmetrized product of one-electron states, can be studied by viewing the pair as a single compound particle, which is characterized by the center-of-mass wave vector $\boldsymbol{K}^{+} = \boldsymbol{k}_3 + \boldsymbol{k}_4$ and the inter-electronic wave vector $\boldsymbol{K}^{-} = (\boldsymbol{k}_3 - \boldsymbol{k}_4)$ , i. e. an internal degree of freedom (cf. Berakdar et al., 1998). Diffraction of the pair by the lattice is governed by the Laue-like condition $\boldsymbol{K}^{+\|} = \boldsymbol{k}_1^{\|} + \boldsymbol{k}_2^{\|} + \boldsymbol{g}^{\|}$ , where $\boldsymbol{g}_{\|}$ is a surface reciprocal lattice vector. Only the center-of -mass wave vector of the

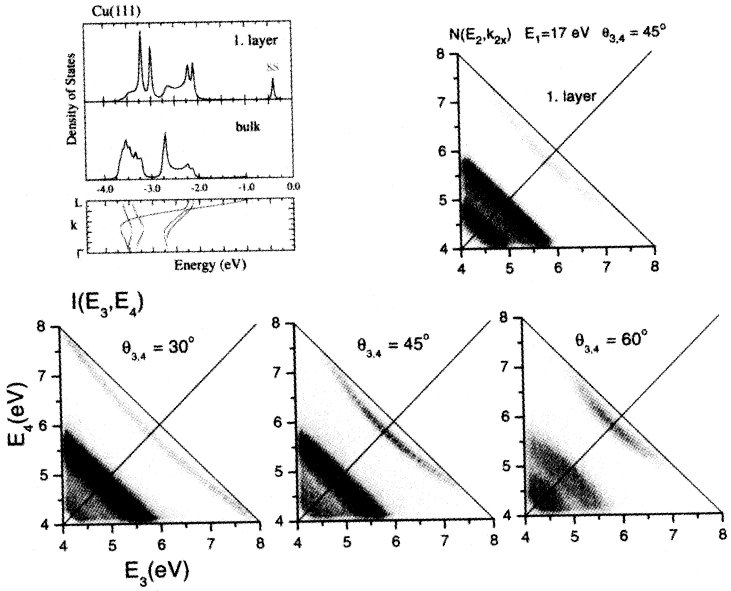


*Figure 4* (e,2e) vision of the sp-surface state on Cu(111). *Upper left-hand panel*: density of states in surface and bulk mono-atomic layer for surface-parallel momentum together with bulk band structure along $\Gamma$–$L$. Note the surface state peak SS at -0.4 eV, i.e. 0.4 eV below the Fermi energy. *Upper right-hand panel*: $\boldsymbol{k}^{\parallel}$-resolved valence electron density of states in the the surface layer. *Lower panels*: calculated (e,2e) intensities in the symmetric coplanar geometry with normal incidence of a 17 eV primary electron and polar detection angles $\theta_3 = \theta_4$ (30°, 45° and 30° as indicated) of the two outgoing electrons (cf. Gollisch et al., 2000)

pair enters in this condition. The above is equivalent to the diffraction of a fictitious particle located at the pair's center of mass. While $\boldsymbol{K}^+$ thus determines the positions of the diffraction peaks, their height and shape is controlled by the inter-electronic correlation. This is illustrated by the measured and calculated cross sections in Fig. 5. The asymmetry between $K_x^+$ and $-K_x^+$ is due to the off-normal incidence of the primary beam, i.e. a nonzero $k_1$ in the above diffraction condition.

In a more quantitative investigation of Coulomb pair correlation effects, (e,2e) cross section distributions from the W(001) surface were calculated using the dynamical screening model outlined in Section 2 and compared to their counterparts calculated without Coulomb correlation (Berakdar et al., 1999). While the modifications of fixed-geometry distributions (like the one shown in Fig. 2) were in general fairly modest, a drastic effect was found for a set-up, in which the detection direction of one electron is fixed and that of the other sweeps over the entire

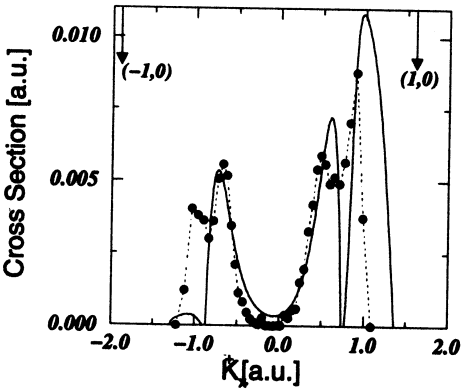


*Figure 5* (e,2e) from Fe(110) with unpolarized primary electrons of energy 50 eV incident in the $(xz)$ plane at polar angle $\theta_1 = 5°$. The two detectors are in the same plane at azimuthal angles 0 and 180° and polar angles 50° and 35°. The experimental (fat dots with a broken line to guide the eye) and theoretical (solid line) cross section is shown as a function of the surface-parallel component $K_x^+$ of the electron pair momentum at fixed pair energy $E_3 + E_4 = 44$ eV. (From Berakdar et al., 1998).

hemisphere. We show this in Fig. 6. Without correlation, the emission probability is seen (cf. left-hand panel of Fig. 6) to be maximal when the two electrons escape into the same direction and with the same velocity. This unphysical result is remedied by the pair interaction (cf. right-hand panel of Fig. 6) which carves a considerable 'pair correlation hole' around the position where electrons are close to each other in velocity space. For regions where the two electrons emerge with diverging directions, the effect of the pair correlation becomes less and less visible.

In the above cases, the primary beam is unpolarized and the (e,2e) cross section I is therefore the average over the cross sections $I^+$ and $I^-$ (cf. Section 2). Since spin polarization effects due to spin-orbit interaction and magnetic exchange interaction are abundant in LEED and photoemission, they must occur also in (e,2e) which involves the same types of one-electron states. For a non-magnetic system (W(001), in which spin-orbit coupling is strong because of its large $Z = 74$) the dependence of the (e,2e) cross section on the spin orientation of the primary electron was extensively investigated by numerical calculations and symmetry considerations (Gollisch et al., 1999). A typical result is shown in Fig. 7. The right-hand contour plot reveals a richly structured intensity difference distribution, which is antisymmetric with respect to the $E_3 = E_4$ diagonal, i. e. changes sign upon interchanging the two detected electron energies. This can readily be understood from the symmetry

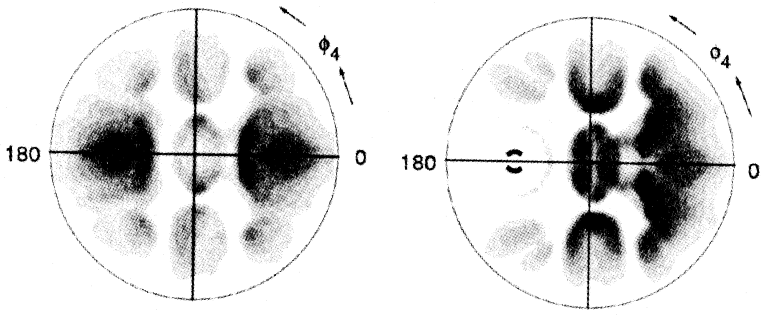


*Figure 6* Calculated (e,2e) angular distribution from W(001) for primary electrons of energy 17.2 eV incident at polar angle $\theta_1 = 88°$ (grazing incidence) and azimuthal angle $\varphi_1 = 0°$. The outgoing electrons have energies $E_3 = E_4 = 6$ eV. One detector is in a fixed direction defined by $\theta_3 = 47°$ and $\varphi_3 = 180°$, and the other scans over the angles $\theta_4$ and $\varphi_4$, which correspond to the radial and angular coordinates in the contour plots. The Coulomb pair correlation is switched off in the left-hand panel and taken into account according to eq. (1) in the right-hand panel. The broken circle around $\theta_4 = 47°$ and $\varphi_4 = 180°$ marks the direction of parallel escape of the two electrons, i. e. the centre of the 'pair correlation hole'. (From Berakdar et al., 1999).

of the set-up. In the lower part of Fig. 7 energy sharing curves are seen to reach asymmetry values up to 30%. With the aid of additional calculations, in which spin-orbit coupling was selectively switched off in the four one-electron states, spin-orbit coupling in the valence state was identified as main source of the asymmetry.

For spin-polarized (e,2e) from a ferromagnetic Fe(110)surface we show in Fig. 8 a recent experimental energy sharing curve of the asymmetry $A$ together with its calculated counterpart. The energies have been chosen such that the relevant valence electron energy $E_2$ is within about 0.5 eV from $E_F$. For equal energies of the outgoing pair, i. e. valence electrons with $\boldsymbol{k}_2^{\parallel}$, $A$ is seen to be positive with a maximum close to 20%. This may seem surprising at first glance, since for $E_2$ near $E_F$ and $\boldsymbol{k}^{\parallel} = 0$ the density of states (trace of the spectral function, cf. above eq. (1)) is larger for minority spin than for majority spin and the spin polarization $P_2(E_2, \boldsymbol{k}_2^{\parallel}) = (N(E_2, \boldsymbol{k}_2^{\parallel}, \uparrow) - N(E_2, \boldsymbol{k}_2^{\parallel}, \downarrow)/(N(E_2, \boldsymbol{k}_2^{\parallel}, \uparrow) + N(E_2, \boldsymbol{k}_2^{\parallel}, \downarrow)$ is hence negative. An explanation has been given with the aid of the factorization $A = -P_2\, A^{\mathrm{scatt}}$, where $A^{\mathrm{scatt}}$ is defined as the relative difference between the singlet and triplet partial cross sections (For details see Berakdar, 1999). For equal energies of the outgoing electrons, the symmetry of the present set-up dictates that the triplet cross section vanishes, i. e. $A^{\mathrm{scatt}} = 1$ and hence $A = -P_2$. The above is strictly valid only in the absence of spin-orbit coupling, but can be

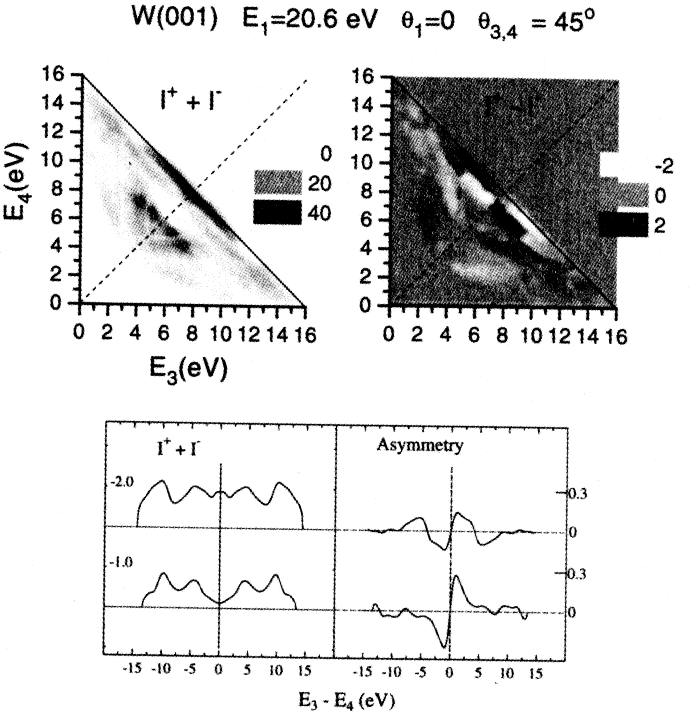


*Figure 7* (e,2e) from W(001) calculated for spin-polarized (along y) primary electrons of energy $E_1 = 20.6\ eV$ at normal incidence and spin-averaged detection of detection of the outgoing electrons in the $(xz)$ plane at polar angles $\theta_3 = \theta_4 = 45°$. The two contour plots represent the sum and the difference of the intensities $I^+$ and $I^-$. The bottom panel shows energy sharing curves of $I^+ + I^-$ (left) and of the asymmetry $A = (I^+ - I^-)/(I^+ + I^-)$ involving valence electrons with energies 1.0 eV and 2.0 eV below the Fermi energy (cf. Gollisch et al., 1999).

expected to hold in good approximation also in its presence. With the extreme surface sensitivity of (e,2e) (cf. above), spin polarized (e,2e) spectroscopy thus offers the possibility of directly mapping the energy- and parallel-momentum resolved spin polarization in the surface layer of a ferromagnet.

## 4. ($\gamma$,2e) RESULTS

Compared to (e,2e), ($\gamma$,2e) from surfaces is still in an early stage of infancy, with the first experimental success reported only two years ago (Herrmann et al., 1998). In Fig. 9 we show measured and calculated energy sharing curves obtained for the (001) surfaces of Cu and Ni, with the valence electron energy very close to the Fermi energy. Calculations

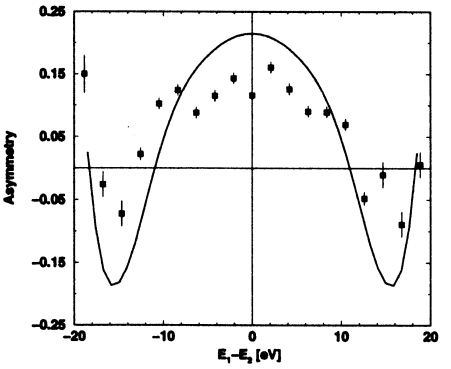


*Figure 8* Measured and calculated (e,2e) spin asymmetry A from ferromagnetic Fe(110) (with magnetization $M$ parallel to the surface along the y axis) as a function of the energy sharing $(E_3 - E_4)/(E_3 + E_4)$ for a fixed total energy $(E_3 + E_4) =$ 21 eV. The normally incident primary electrons of energy 26 eV are spin-polarized anti-parallel/parallel to $M$ (i. e. parallel/anti-parallel to the majority spins of the target) with a polarization degree of 65 %. The electron detectors are in the $(xz)$ plane at polar angles $\theta_3 = \theta_4 = 40°$. The theoretical results are averaged over the angular resolution of the detectors. (From Berakdar, 1999).

of the 2e-photocurrent due to the direct excitation process were performed with a jellium-type initial state without Coulomb correlation and a correlated final two-electron state which does not incorporate multi-

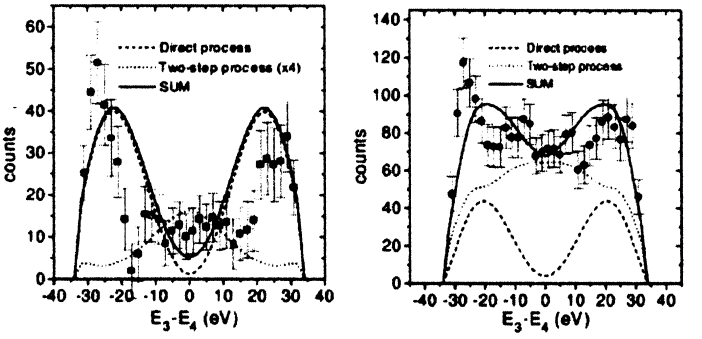


*Figure 9* ($\gamma$,2e) energy sharing distributions from Cu(001) (left-hand panel) and Ni(001) (right-hand panel) due 45 eV photons incident normal to the surface. The experimental data (Herrmann et al., 1999) are for electron pairs with sum energies $E_3 + E_4$ between 33 eV and 35 eV. The theoretical curves (due to Berakdar, shown in Herrmann et al., 1999) (for sum energy 34 eV) show the contributions from the direct excitation process (dashed lines) and the two-step process (dotted lines) together with their sum (solid lines).

ple elastic scattering by the lattice (Berakdar, 1998). Having cast the transition matrix element into the form $\boldsymbol{E} \cdot (\boldsymbol{k}_3 + \boldsymbol{k}_4) L$, where $L$ is a complicated function of $\boldsymbol{k}_3$ and $\boldsymbol{k}_4$, the cross section for $E_3 = E_4$ is seen to vanish in the case of normal incidence. Hence a deep minimum for equal energy sharing. The discrepancy of this result for the direct excitation process with the experimental data is remedied by including the two-step process in which a single electron is photo-excited and collides with another valence electron. The sum of the two contributions is seen to be in general agreement with experiment. The minimum at equal energies is significantly deeper for Cu than for Ni. For some further theoretical results we refer to Fominykh et al., 2001.

## 5. OUTLOOK

A brief summary given in the abstract, we address in this final section the probably strongest challenge for future theoretical work, the Coulomb correlation between the two detected electrons and in the case of ($\gamma$,2e) also between the two initial-state electrons. In (e,2e) it is possible to choose geometrical arrangements, in which pair correlation plays only a minor role and single-quasiparticle properties can be probed, in particular the surface-layer density of states $N(E, \boldsymbol{k}^{\parallel})$ and the spin polarization $\boldsymbol{P}(E, \boldsymbol{k}^{\parallel})$ at the surface of a ferromagnet. In contrast, the direct ($\gamma$,2e) process owes its very existence to correlation and a computationally viable realistic treatment is indispensable.

## References

Berakdar, J. (1998). Emission of correlated electron pairs following single-photon absorption by solids and surfaces. *Phys. Rev. B*, 58:9808.

Berakdar, J. (1999). Probing the spin polarization in ferromagnets. *Phys. Rev. Lett.*, 83:5150.

Berakdar, J., Gollisch, H., and Feder, R. (1999). Pair correlation in two-electron emission. *Sol. State Commun.*, 112:587.

Berakdar, J., Samarin, S. N., Herrmann, R., and Kirschner, J. (1998). Manifestations of electronic correlations in the diffraction of electron pairs from crystals. *Phys. Rev. Lett.*, 81:3535.

Feder, R., editor (1985). *Polarized electrons in surface physics.* Advanced Series in Surface Science. World Scientific, Singapore.

Feder, R., Gollisch, H., Meinert, D., Scheunemann, T., Artamonov, O. M., Samarin, S. N., and Kirschner, J. (1998). Low-energy $(e, 2e)$ spectroscopy from the W(001) surface: Experiment and theory. *Phys. Rev. B*, 58:16 418.

Fominykh, N., Henk, J., Berakdar, J., Bruno, P., Gollisch, H., and Feder, R. (2000). Theory of two-electron photoemission from surfaces. *Sol. State Commun.*, 113:665.

Fominykh, N., Henk, J., Berakdar, J., Bruno, P., Gollisch, H., and Feder, R. (2001). Two-electron photoemission from surfaces. Article in this volume.

Gollisch, H., Scheunemann, T., and Feder, R. (2000). Theoretical study of (e,2e) from surface states. To be published.

Gollisch, H., Xiao, Y., Scheunemann, T., and Feder, R. (1999). Spin-polarized low-energy (e, 2e) spectroscopy of non-magnetic surfaces. *J. Phys.: Condens. Matt.*, 11:9555.

Halilov, S. V., Tamura, E., Gollisch, H., Meinert, D., and Feder, R. (1993). Relativistic Green function theory of layer densities of states and photoemission from magnetic compounds. *J. Phys.: Condens. Matt.*, 5:3859.

Herrmann, R., Samarin, S., Schwabe, H., and Kirschner, J. (1998). Two electron photoemission in solids. *Phys. Rev. Lett.*, 81:2148.

Herrmann, R., Samarin, S., Schwabe, H., and Kirschner, J. (1999). Two-electron photoemission processes in the valence bands of solids. *J. Phys. (Paris) IV*, 9:127.

Kirschner, J. and Samarin, S. (2001). Two-electron spectroscopy of solid surfaces. Article in this volume.

Meinert, D. (2000). *Relativistische Theorie der Elektronen-Koinzidenz-Spektroskopie für Festkörperoberflächen.* PhD thesis, Theoretische Festkörperphysik, Universität Duisburg.

Stefani, G. (2001). Emission of electron pairs from surfaces: The grazing impact geometry. Article in this volume.

Vos, M., Kheifets, A. S., Weigold, E., Canney, S. A., Holm, B., Aryasetiawan, F., and Karlsson, K. (1999). Determination of the energy-momentum densities of aluminium by electron momentum spectroscopy. *J. Phys.: Condens. Matt.*, 11:3645.

Weigold, E. (2001). (e, 2e) studies of condensed matter and surfaces—A review of recent results. Article in this volume.

Weigold, E. and McCarthy, I. E. (1999). *Electron Momentum Spectroscopy.* Kluwer Academic/Plenum Publishers.

Whelan, C. T. and Walters, H. R. J., editors (1997). *Electron Coincidence Studies of Electron and Photon Impact Ionization.* Plenum, New York.